Ore Geology Reviews 89 (2017) 1–14

Contents lists available at ScienceDirect

Ore Geology Reviews

journal homepage: www.elsevier.com/locate/oregeo

Prospectivity mapping for "Zhuxi-type" copper-tungsten polymetallic deposits in the Jingdezhen region of Jiangxi Province, South China

Chengbin Wang [a,b], Jianfeng Rao [c], Jianguo Chen [a,*], Yongpeng Ouyang [c], Shuaijun Qi [a,d], Qiang Li [c]

[a] State Key Laboratory of Geological Processes and Mineral Resources & Faculty of Earth Resources, China University of Geosciences, Wuhan 430074, China
[b] Department of Computer Science, University of Idaho, Moscow, ID 83844, USA
[c] 912 Party of Jiangxi Bureau of Geology and Mineral Exploration, Yingtan 335001, China
[d] Institute of Mineral Resources, Chinese Academy of Geological Sciences, Beijing 100037, China

ARTICLE INFO

Article history:
Received 30 May 2016
Received in revised form 18 May 2017
Accepted 22 May 2017
Available online 26 May 2017

Keywords:
Prospectivity mapping
Zhuxi copper-tungsten deposit
Derivative norm
Weights-of-evidence
Singularity

ABSTRACT

The Zhuxi deposit is the largest copper-tungsten polymetallic deposit in the world and is in Jiangxi Province in South China. The ore body is characterized by hydrothermal-vein deposits of copper, lead, and zinc minerals at shallow levels, skarn deposits of tungsten and copper minerals at middle levels, and altered-granite-hosted copper and tungsten minerals at depth. Such metallogenic systems are typically intrusion-related. The intrusive granites related to the Zhuxi polymetallic deposit have been dated at 152.9 Ma to 146.9 Ma. The intrusions provided the thermal energy and the source material for the ore mineralization. Skarns mineralization, the main type of ore mineralization, developed in the contact zone of Carboniferous-Permian formations with the granites. Nappe structures changed the dip of the ore bodies from steep in the top part to gentle in the bottom. NE-trending faults provided the fluid pathways and controlled the geological framework and distribution of ore deposits on a regional scale. In this study, recognition exploration criteria were analyzed based on a mineral deposit model and the geological setting. Extraction of favorable geological information and GIS-based data-integration methods were used for mineral-prospectivity mapping of Zhuxi-type polymetallic deposits. Buffering analysis was employed to extract structural information (e.g. faults) and lithologic or stratigraphic information (e.g. granites or geologic units). The singularity method and spatially weighted principal component analysis were used to enhance and delineate geochemical anomalies. The derivative norm was utilized to extract magnetic-gradient anomalies associated with intrusive granites. Student *t*-test of weights-of-evidence (WofE) proved to be an effective way to optimize threshold values for binarization of variables as evidence layers by evaluating the spatial correlation between known deposits and geological variables. The posterior probabilities of WofE gave a relative estimation of mineralization potential. Areas delineated by high posterior probability had much higher potentiality for the discovery of new deposits where had none had been found yet.

1. Introduction

Jiangxi Province is an important tungsten province in China as well as in the world. Previous studies concluded that world-class tungsten orebodies (e.g. Xihuashan, Dajishan, Yaogangxian deposits) developed in the southern part of Jiangxi Province, within the Nanling tungsten-tin metallogenic belt (Li et al., 1986; Liu et al., 2014a; Mao et al., 2007; Peng et al., 2006). The northern part of Jiangxi Province, which adjoins the middle-lower Yangtze River Valley area, is well known for copper–gold–molybdenum–iron porphyry and skarn ore bodies. With the development of Chinese geological and mineral resources prospecting in recent years, two very large tungsten deposits, Zhuxi and Dahutang, were discovered in the northern Jiangxi Province. The discovery of these world-class tungsten deposits subverted the long-held spatial distribution pattern of "tungsten in the south and copper in the north" within Jiangxi Province and resulted in the establishment of the "North Yangtze tungsten belt" (Mao et al., 2012).

Mineral-prospectivity mapping is based on a mineral predictive model rather than on empirical data from mapping mineral deposits (Asadi et al., 2015). The model analyzes relevant recognition criteria for mineral deposits and synthesizes favorable evidence layers from multi-source data at a given scale (Bonham-Carter, 1994; Carranza, 2009; Carranza and Laborte, 2014). In the past few decades, numerous methods have been proposed and used in

* Corresponding author.
E-mail address: jgchen@cug.edu.cn (J. Chen).

http://dx.doi.org/10.1016/j.oregeorev.2017.05.022
0169-1368/

mineral-prospectivity mapping, which can be grouped into two classes: knowledge-driven and data-driven mineral predictive models. The knowledge-driven model uses the expert knowledge of mineral-deposit exploration to estimate metallogenetic potentiality in a given geological setting (Abedi et al., 2013; Carranza, 2008; Rodriguez-Galiano et al., 2015). It is suitable for green field modelling, which predicts mineral deposits where few or no orebodies are known to exist (Carranza and Laborte, 2014; Lusty et al., 2012). In contrast, the data-driven model is used in brownfield exploration, which delineates new targets for further exploration based on existing data for areas where orebodies are already known to exist. Weighted parameters are assigned to individual evidence layers to quantify the spatial association between known mineral deposits and geological features. The weights-of-evidence (WofE) model is a quantitative data-driven model based on the log-linear form of the Bayesian probability model to quantify spatial association (Agterberg and Cheng, 2002; Bonham-Carter, 1994; Cheng, 2008). It allows the users to calculate WofE layers and apply posterior probability mapping to mineral exploration.

Data from geochemical surveys and geophysical exploration were mapped with the geology of the Jingdezhen region (northern Jiangxi Province) at a scale of 1:50, 000 scale, and the mineral deposit model was run. In the study area, the resulting discovery of the intrusion-related Zhuxi copper-tungsten polymetallic deposit inspired a new guideline for mineral exploration. In this paper, we review the Zhuxi mineral deposit model and the orebody's geological setting, analyze recognition criteria for regional exploration based on the mineral predictive model instead of the mineral deposit model, calculate posterior probability and delineate prospectivity targets by the WofE model.

2. Geology

2.1. Geological setting and study area

In terms of geological structure, South China consists of the Yangtze Craton in the northwest and the Cathaysia Block in the southeast. These two parts were assembled by a subduction-collision event at ca. 970 Ma (Li and Mcculloch, 1996). The event also resulted in the formation of Jiangnan Orogen between the Yangtze Craton and the Cathaysia Block (Wang et al., 2012). The approximately 1500-km long E-NE-trending Jiangnan Orogen consists of Precambrian meta-sedimentary sequences and igneous rocks (Huang and Jiang, 2014; Wang et al., 2006, 2015; Zhao, 2015; Zhao and Cawood, 1999). The orogen basement comprises two series of metasedimentary strata in unconformable contact with sub-greenschist to greenschist facies rocks (Zhao, 2015; Zhou et al., 2009). The metamorphic transformation from sedimentary rock to metasedimentary rock occurred in the Neoproterozoic (Gao et al., 2008, 2012; Wang and Zi, 2007). The most recently discovered tungsten deposits are distributed in the Jiangnan Orogen (Fig. 1) rather than the metallogenic province of the middle to lower Yangtze River Valley.

The study area is in the Taqian-Fuchun-Jingdezhen district (TFJD), which includes approximately 2000 km^2 of the northeastern part of the Jiangnan Orogen (Figs. 1 and 2). The Zhuxi polymetallic deposit is in the Neopaleozoic shallow marine carbonate-rock basin of the Jiangnan Orogen. The metallogenic province of the middle to lower Yangtze River Valley, characterized by copper-gold-molybdenum–iron porphyry and skarn ore deposits, is in the northeast of the study area. The well-known Dexing copper and Dahutang tungsten deposits have a geological setting that is similar to that of the Zhuxi tungsten deposit. They are both located in the northeastern part of Jiangnan Orogen (Fig. 1).

2.2. Lithostratigraphy

The oldest rock in the TFJD belongs to the Neoproterozoic Shuangqiaoshan Group, which consists of low greenschist facies rocks formed in the back-arc basin from ca. 850 Ma to ca. 820 Ma (Gao et al., 2008, 2012; Han et al., 2016; Wu et al., 2005). Shuangqiaoshan Group, which has an extremely variable strata sequence, is composed of pelitic-sandy sedimentary rock (greater than 500 m thick) with volcanic interlayers (Wang et al., 2008). It includes sericitized phyllite, sandy phyllite, sericitized killas and metamorphosed tuff. The Shuangqiaoshan Group, which forms the basement of Taqian-Fuchun synclinal basin, is characterized by the enrichment of Cu, As, Sb, Be, Pb, Sn, W, Mo, V, Li, Cd, and Zn in the Taqian district. The concentrations of As, Sb, W, Cd are 60 to 150 times higher than Clarke values (Hu, 2015). In general, the Shuangqiaoshan Group is regarded as having provided source materials for some ore deposits, such as the Jinshan gold deposit, Dexing copper deposit, and the Yinshan silver polymetallic ore deposit (Hua et al., 1993; Wan, 1995; Wei, 1996; Xi and Liao, 1997).

The unconformable boundaries between the Shuangqiaoshan Group and the overlying Carboniferous strata (approximately 200–300 m in thickness) extend along a NE-trending graben basin. Most of the unconformable boundaries were obscured by later NE-trending thrust faults. The Carboniferous strata can be further divided into five formations from oldest to youngest: the early Carboniferous Yunshan, Zhongpeng, Zishan Formations and the late Carboniferous Laohudong and Huanglong Formations. Early Carboniferous strata are a sedimentary sequence from conglomerate at the bottom to fine-grained sandstone with limestone and shale interlayers at the top. The late Carboniferous strata consist of limestone and dolomite deposited in a tidal-flat environment. The Huanglong Formation is relatively more enriched in Cu, W, and Zn (Chen et al., 2012).

During the Permian, a sedimentary sequence of limestone, chert, mudstone and clastic rocks was formed in an inland-sea environment. The sequence comprises the early Permian Liangshan, Qixia, Xiaojiangbian, Maokou and Mingshan Formaitons, and the late Permian Leping and Changxing Formations.

Triassic to Cretaceous rocks are scattered across the study area. During the Triassic, Qinglong Formation and Anyuan Group were deposited in inland sea platform and paralic shallow marine environments, respectively. The Duojiang Formation of Upper Triassic to Lower Jurassic is a sedimentary sequence of clastic rocks and shales with thin coal seams. The Linshan Group of Jurassic is a continental sequence of conglomerate, quartz sandstone and siltstone. The Cretaceous sediment sequence includes red sandstone, and siltstone with mudstone interlayers formed in an oxidation environment.

2.3. Intrusive rocks

In the study area, an S-type granite was intruded into the Taqian-Fuchun synclinal basin along the NE trending faults in an extensional and post-collisional environment (Hu, 2015; Li et al., 2014). The exposed granite dykes and stocks are compositionally categorized as porphyritic granodiorite, granite porphyry, granodiorite, biotite granite and muscovite granite, which were dated at 152.9 Ma to 146.9 Ma by using the zircon U-Pb method (Chen et al., 2015; Li et al., 2014; Su, 2014; Wan et al., 2015). The Cu, Mo, W, Zn and Ag mineral systems have a close spatial and genetic relationship with the granites. There are also some mafic and intermediate-felsic dykes of unknown age and lamprophyre veins dated at 160.3 Ma along the NE trending faults (Liu et al., 2014b).

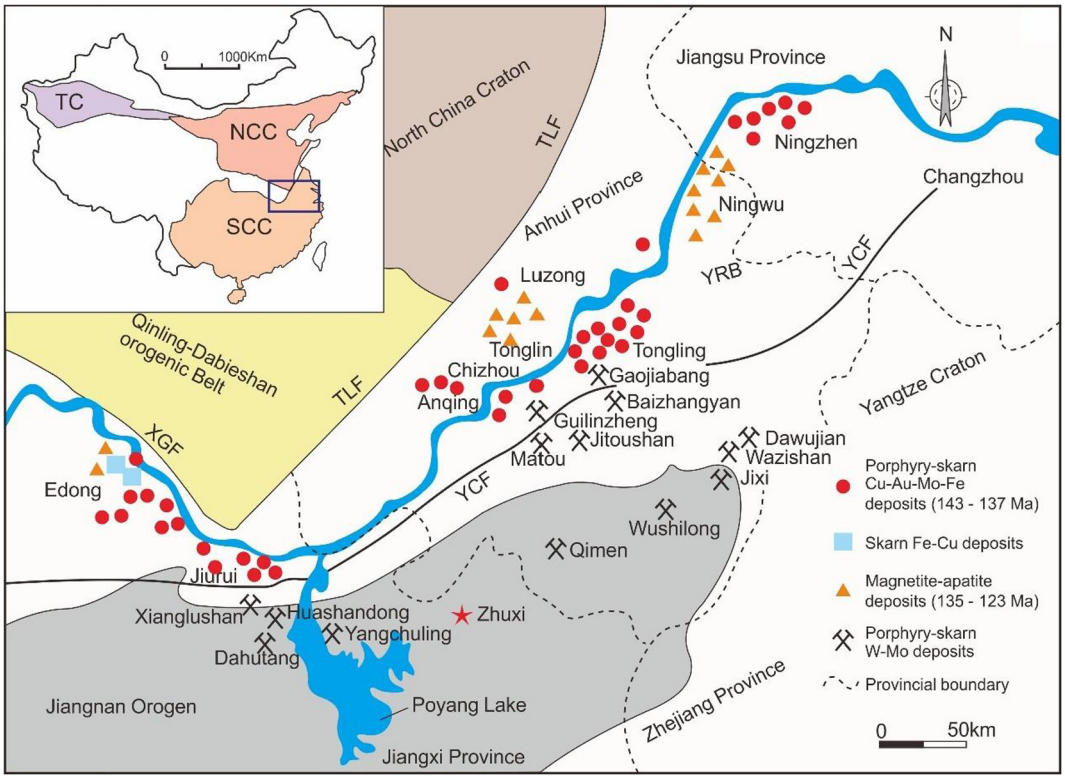

Fig. 1. Geological map showing the distribution of mineral deposits in Jiangnan Orogen and Yangtze River Belt (YRB). YCF, Yangxing-Changzhou Fault; TLF, Tancheng-Lujiang Fault; XGF, Xiangfan-Guangji Fault; NCC, North China Craton; SCC, South China Craton; TC, Tarim Craton (Mao et al., 2013).

2.4. Structural geology

Neoproterozoic and Mesozoic tectonic activities mainly affected the supracrustal faults, intrusive rocks and mineralization. They also played a key role in forming the present-day structural framework (Yang et al., 1998, 2009). Neoproterozoic tectonic activity characteristically produced tight linear folds, large-scale nappe structures and ductile shear zones (Shu et al., 1995; Xu et al., 1992). Mesozoic tectonic activity characteristically produced folds in overlying rocks, brittle fractures and rift basins (Shu et al., 2008). Mesozoic lithosphere extension produced igneous rocks (granitic and volcanic) in a rift basin in the northern part of Jiangxi Province and resulted in large-scale mineralization (Jiang et al., 2006; Mao et al., 2004; Wang and Shu, 2012; Zhou et al., 2006).

Neoproterozoic lithologies were overthrust from north to south onto the sedimentary sequences along the NE-trending Taqian-Fuchun Fault during the Mesozoic. These overthrust basin sediments protected ore-bearing rocks from subsequent erosion (Chen et al., 2012). In the study area, four NE-trending parallel faults controlled the distribution of copper-tungsten polymetallic deposits. Locally, minor E-W or NE-trending faults later intersected these more-dominant NE-trending parallel faults, and these intersections became favorable places for granite intrusion and hydrothermal alteration.

3. Typical mineral deposit model and predictive model

3.1. Mineral deposit model

The Zhuxi orefield is the most studied of any within the TFJD. When it was discovered, it was regarded as a reworked and overprinted sedimentary copper deposit. With the discovery of the underlying ore-bearing intrusive rocks, the Zhuxi orebody became the largest known tungsten deposit in the world. It was reported to contain 2.86 Mt WO_3, 224.4 Kt Cu, and 1.2 Kt Ag (Li and He, 2016). The Zhuxi's mineral reserve of WO_3 is 2.7 times that of the Dahutang tungsten deposit, which previously was considered largest in the world. In this study, the Zhuxi mineral deposit model was reviewed to define predictive model and regional-scale recognition criteria for mineral exploration.

The Zhuxi copper-tungsten polymetallic deposit includes two ore zones (Figs. 2 and 3). The first is the main ore zone, which is a typical skarn tungsten deposit. Skarn mineralization occurred in the alteration zone between the Carboniferous carbonates and the granite. The structurally formed zone between the Neoproterozoic low-grade metamorphic rocks and the Carboniferous Huanglong Formation provided a favorable fluid pathway. The NE-trending orebody dips 30–75° to NW, is 750 m long, and extends greater than 2000 m down dip. Since the orebody was affected by the nappe structures, it is characterized by significant dip change from steep in the top part to gentle in the bottom. The dip angles in the top are generally greater than 60°, whereas the angles are less than 30° in the bottom and middle (Fig. 4). The greatest thickness is 577.9 m with a WO_3 grade of 0.64% (Liu et al., 2013). The orebody is characterized by pervasive veinlet, stockwork and massive structures and is characterized by a mineral assemblage of garnet, tremolite, diopside, wollastonite, serpentine, talc, quartz, calcite, pyrite, scheelite, chalcopyrite, pyrrhotite, and sphalerite. The wall-rock alteration shows significant zonation from the granites to the carbonate rocks (Fig. 4) (Hu, 2015).

The other ore zone of the Zhuxi deposit is characterized by hydrothermal-vein type mineralization. Formed along the contact between the Huanglong Formation and the Maokou-Chuanshan Formations (Chen et al., 2015), these orebodies are within a distance of 30–40 m away from the strata boundaries and are lenticular or are confined to veins (Wu et al., 2015). Additionally, len-

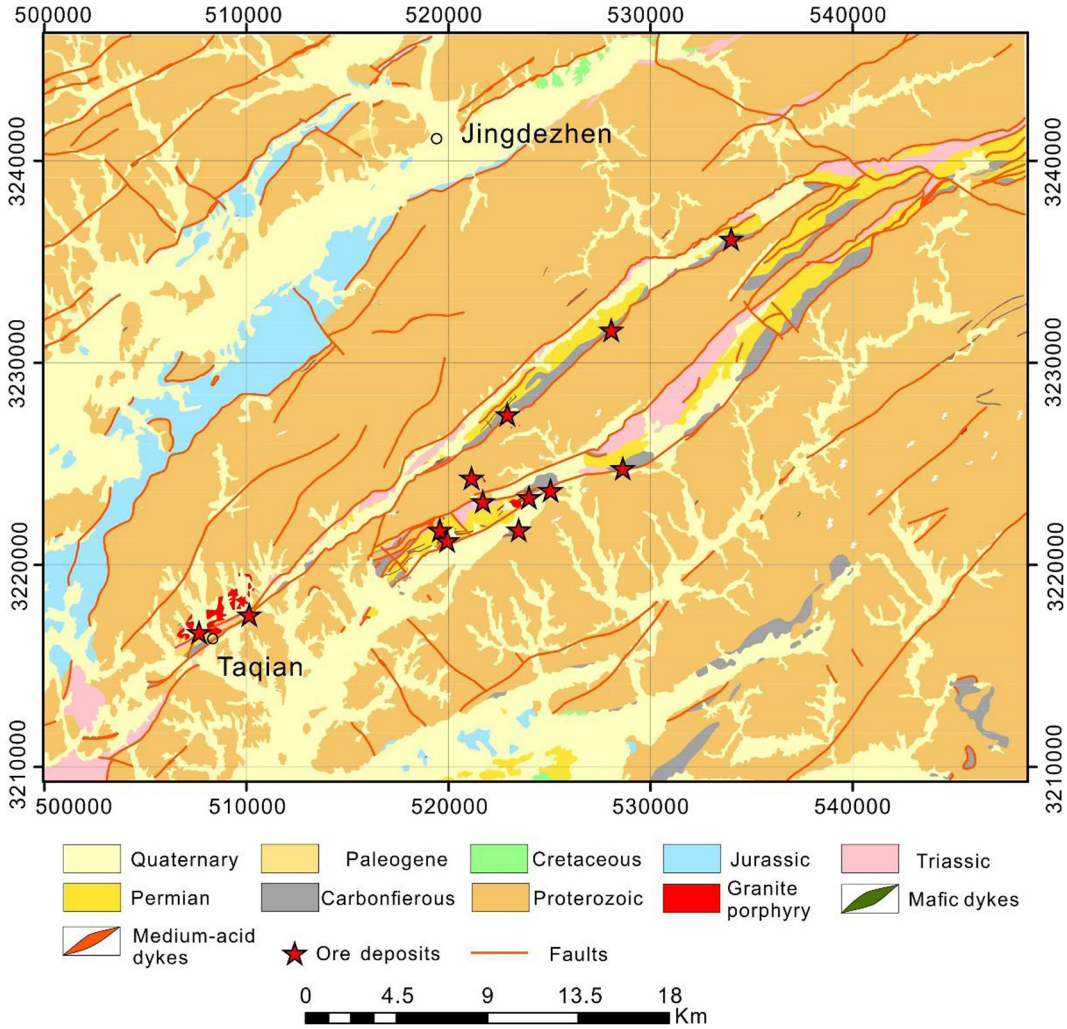

Fig. 2. Geological map of Taqian-Fuchun-Jingdezhen district (TFJD) showing the known mineral deposits (occurrences) and geological features.

ticular orebodies hosted in altered granite occur below the surface at depths of greater than 800 m. These deposits have a mean WO_3 grade of 0.16% (Hu, 2015).

In the Zhuxi orefield, intrusive granites are S-type, produced by crustal melting mixed with mantle material (Hu, 2015). Scheelite Sm-Nd dating determined an isochron age of 144 ± 5 Ma for the mineralization (Hu, 2015). Fluid-inclusions research showed that homogenization temperatures of the skarn stage are occurred in the range of 231–359 °C, the retrograde skarn stage is in the range of 167–355 °C, and the quartz-sulfide stage is in the range of 114–351 °C (Li et al., 2014). H-O-S isotopes indicated that the ore-forming fluid originated from magma (Hu, 2015).

3.2. "Zhuxi-type" copper-tungsten predictive model

A mineral deposit model is not the same as a mineral predictive model. The China Geological Survey (2010) classified mineral predictive types into sedimentary, volcanic, intrusion-related, metamorphic, composite-endogenous, and strata-bound-endogenous types. The intrusion-related mineral predictive type encompasses all mineral deposits related to the intrusion-related mineral systems. It includes mineral deposits located within the intrusive rock (e.g. magmatic and porphyry deposits), the contact zone (e.g. skarn deposits), and area influenced by hydrothermal fluids generated by intrusive rock (e.g. high-temperature hydrothermal mineral deposits) (Xiao et al., 2009).

Wu et al. (2015) modelled the Zhuxi mineral deposit as having three components: 1) mineralization characterized by hydrothermal-vein type copper, lead, and zinc deposits at shallow depths; 2) mineralization characterized by skarn-type tungsten and copper deposits at intermediate depths; and 3) mineralization characterized by altered-granite-type copper and tungsten deposits at depth. The copper mineralization is predominantly in the northeastern part of the orefield, whereas the tungsten mineralization is predominantly in the southwestern part (Chen et al., 2015). At the orefield scale, the Zhuxi mineral deposit exhibits several mineralization types. They share some ore-controlling features, but each type also has unique characteristics. Several types have in common a spatial and genetic relationship with intrusive granite. Therefore, we consider the Zhuxi mineral deposit to be the intrusion-related type, in accordance with the China Geological Survey (2010) classification.

In the past decades, 13 hydrothermal polymetallic deposits (or occurrences) have been found in the TFJD. As is true of the Zhuxi mineral deposit, they are controlled by NE-trending faults, are hosted by Carboniferous-Permian limestone formations, are characterized by geochemical anomalies and magnetic transition zone, and are related to (concealed) granite intrusions. Although they are only small- to medium-mineral deposits if classified into the different specific types according to the geological features present, they each have the potential to be a large mineral deposit if the concealed intrusive rock were to be discovered. Therefore, these

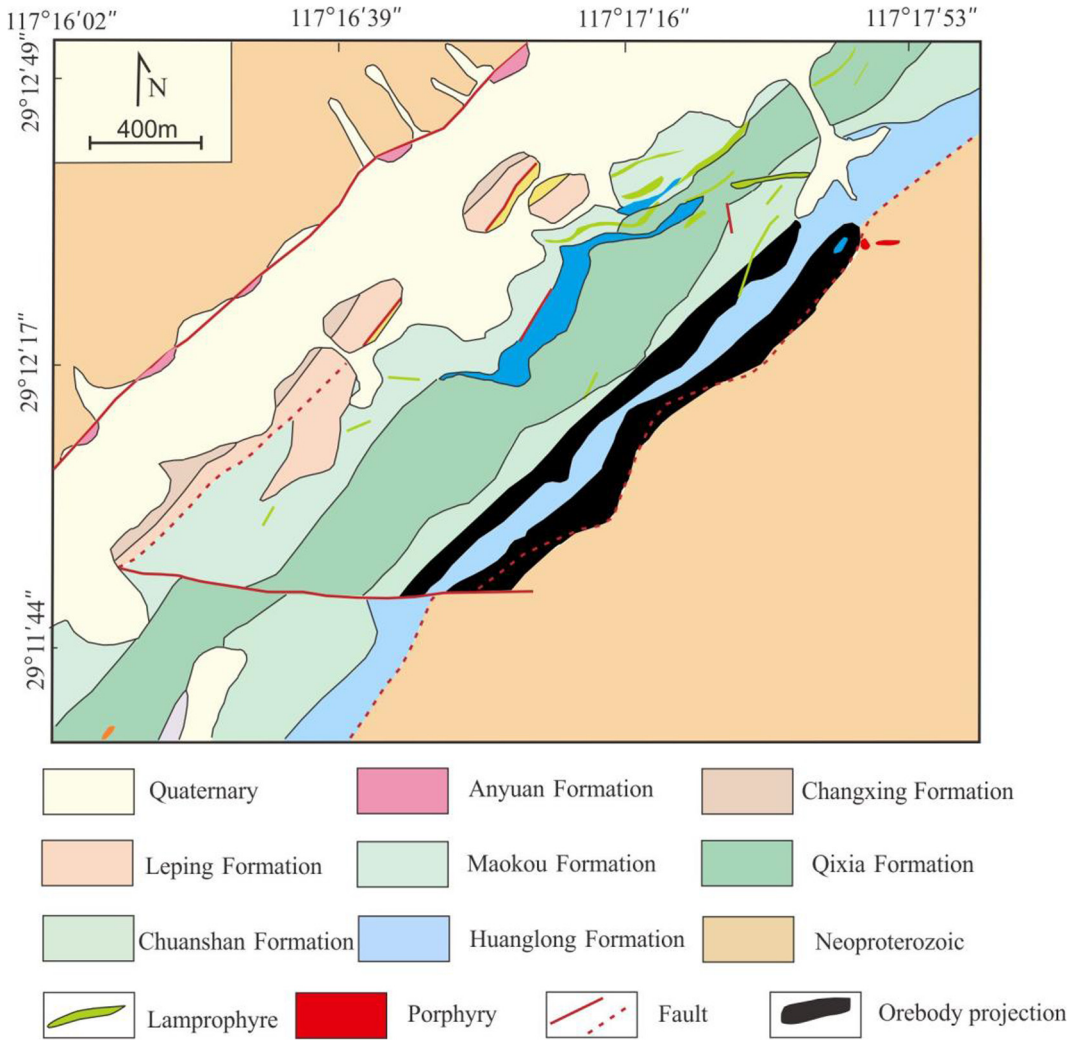

Fig. 3. Simplified geological map of Zhuxi copper-tungsten deposits (modified from Chen et al., 2015).

deposits were also categorized as intrusion-related type, as were the Zhuxi mineral deposits. Because the Zhuxi deposit has been researched more than any other in the TFJD, we have named this predictive type the "Zhuxi-type" intrusion-related deposit.

Research on the mineral deposit genesis and deposit type is also necessary for prospectivity mapping. The mineral deposit model can be used to improve the understanding about ore-controlling factors and ore deposit indicators. At the orefield scale, the mineral types can be divided into skarn and hydrothermal-vein and altered-granite types. There are some detailed differences in terms of ore-controlling factors at the orefield scale, such as the ore-forming space. In regional prospectivity mapping, different mineralization types have a spatial correlation, and share some similar ore-controlled factors and predictive indicators. Therefore, we regarded different mineralization types in the Zhuxi mineral orefield as a research objective, and we conceptually scaled up the mineral deposit model to do regional-scale predictive modelling according to the principles of scale equivalence.

4. Datasets and methods

4.1. Datasets

Geological mapping at 1:50, 000 scale, stream-sediment geochemical sampling, and geophysical surveying were carried out by Jiangxi Bureau of Geology and Mineral Exploration. For geochemical analysis, 7403 stream-sediment samples were analyzed for Au, Ag, Cu, Pb, Zn, W, Sn, Mo, Bi, As, Sb, Cr, Co Cd, Hg, Ni, and Ba. The ground magnetic survey was carried out along profiles with 500 m spacing and 100 m reading intervals. A total of 31,126 stations were included. These datasets were registered to the same coordinate system and merged into a multi-sources geological information database using GIS.

4.2. Weights-of-evidence and Student's t-test

WofE is a quantitative data-driven method that uses a log-linear form of the Bayesian probability model (Bonham-Carter, 1994). The WofE method is used to estimate the relative importance of evidence layers for known deposits and to minimize subjective bias (Agterberg et al., 1993; Andrada de Palomera et al., 2014; Lindsay et al., 2014). Weight coefficients W^+ and W^-, which are calculated by conditional probability, indicate the spatial association between evidence layers and known mineral deposits. The detailed description is shown in the following equations.

$$W^+ = \ln \frac{n(E \cap M)/n(M)}{n(E \cap \overline{M})/n(\overline{M})} \quad (1)$$

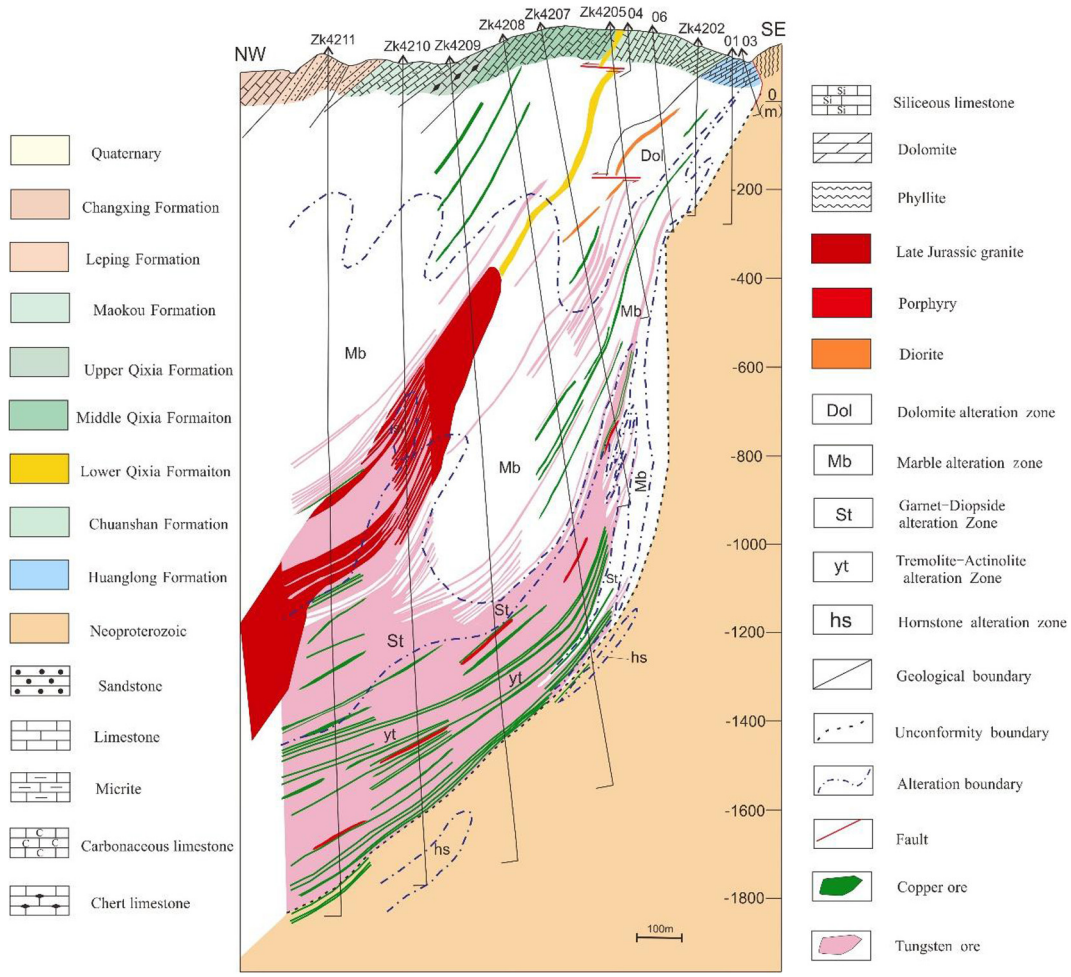

Fig. 4. The L42 geological section of Zhuxi copper-tungsten deposits showing the zonation of mineralization and alteration types (Chen et al., 2015).

$$W^- = \ln \frac{n(\overline{E} \cap M)/n(M)}{n(\overline{E} \cap \overline{M})/n(\overline{M})} \tag{2}$$

where $n(E \cap M)$, $n(E \cap \overline{M})$, $n(\overline{E} \cap M)$, and $n(\overline{E} \cap \overline{M})$ represent the number of unit cells or pixels of $E \cap M$, $E \cap \overline{M}$, $\overline{E} \cap M$,and $\overline{E} \cap \overline{M}$, respectively, on map patterns. M and $\overline{M}$ indicate the presence and absence of known ore deposits. E and $\overline{E}$ indicate the presence and absence of favorable factors (e.g. fault buffering, geochemical anomalies). High positive W^+ values and low W^- values indicate the factors are favorable evidence for the known mineral deposits. Posterior probabilities were calculated by combining weight coefficients using the odds formulation of Bayes' rule (Agterberg et al., 1993; Bonham-Carter, 1994; Lindsay et al., 2014).

An important index to estimate spatial correlation, t-test was developed from contrast of weight coefficients of WofE (Agterberg et al., 1990; Bonham-Carter, 1994). The accepted threshold above which correlation can be considered statistically significant is t-values $\approx$ 1.96 at 95% confidence interval (Agterberg et al., 1990; Bonham-Carter, 1994; Zuo, 2011).

$$t = \frac{C}{S(C)} = \frac{C}{\sqrt{S^2(W^+) + S^2(W^-)}} \tag{3}$$

where contrast $C = W^+ - W^-$, $S(C)$ is the standard deviation of C, $S^2(W^+)$ and $S^2(W^-)$ are the variances of weights (W^+ and W^-), respectively.

4.3. Spatially weighted principal component analysis

Spatially weighted principal component analysis (SWPCA) introduced the spatial-correlation coefficient to principal component analysis (Cheng et al., 2011; Cheng, 2006b). The coefficient is defined by spatial distance, density and intensity associated with mineral deposits. The symmetrical correlation index is calculated by the equation

$$R(x,y) = \frac{\sum w_{ij}(x_{ij} - \overline{x})(y_{ij} - \overline{y})}{\sqrt{\sum w_{ij}(x_{ij} - \overline{x})^2}\sqrt{\sum w_{ij}(y_{ij} - \overline{y})^2}} \tag{4}$$

where $R(x,y)$ is the symmetrical correlation index; x_{ij} and y_{ij} are the geochemical-element contents of samples from location (i,j); $\overline{x}$ and $\overline{y}$ are the weighted mean values of x_{ij} and y_{ij}; and w_{ij} is the spatial correlation coefficient ($0 < w_{ij} < +1$). It is proposed to extract integrated geochemical anomalies based on the mineral-deposits controlling field of the NE-trending faults, thus:

$$w = \begin{cases} 1 & d \leqslant d_{opt} \\ [1 - (d - d_{opt})/d_{\max}]^{\beta} & d_{opt} < d \leqslant d_{\max} \end{cases} \tag{5}$$

where d is the buffering distance of NE-trending faults. The maximum value of d in the study area is 3 km when the buffering region covered the whole study area. d_{opt} is the optimal buffering distance obtained by t-test, for which the buffering region could cover the all deposits and have high correlation between them; β is a positive exponent ($0 < \beta < +\infty$), which determines the decay rate of the

power-law function. More detail regrading Eq. (5) can be found in Cheng et al. (2011) and Xiao et al. (2012).

4.4. Singularity theory

Singularity can be defined as an index used to describe the anomalous behaviors of individual physical processes that generate large material accumulation and energy release within specified spatiotemporal intervals (Cheng, 2006a, 2007, 2008). Singularity is characterized by power law model based on fractal and multifractal theory and has been used to identify weak and local anomalies in geochemical exploration.

In two-dimensional space, the power-law relation (Carranza and Hale, 1997; Cheng, 2007) is expressed by the equation

$$T(A) = cA^{\alpha/2} \tag{6}$$

where $T(A)$ is the total amount in area A; α is the singularity index or the exponent of the power-law relationship; and c is a constant. Considering that the average concentration $\rho(A)$ in A can be expressed as

$$\rho(A) = T(A)/A \tag{7}$$

a similar power-law relationship can be derived:

$$\rho(A) = cA^{\alpha/2-1} \tag{8}$$

If singularity index $\alpha \approx 2$, there is no singularity; if $\alpha < 2$, there is a positive anomaly indicating a concentration enrichment; and if α greater than 2, there may be a concentration depletion.

4.5. Derivative norm

Intrusive granites provide both favorable source material and related thermal energy conducive to forming mineral deposits. The setting of such intrusion-related orebodies has been found to be represented by a magnetic gradient surrounding the intrusive-granite host (Wang et al., 2013). In this work, a derivative norm was proposed and used to highlight magnetic anomalies for mineral prospecting. The method is represented by the equation

$$|Der| = \rho \times \sqrt{Der_x^2 + Der_y^2} \tag{9}$$

where Der_x and Der_y are horizontal derivatives in the directions X and Y, and ρ is a constant (set as 10,000 in this study) used to amplify signal and avoid numeric overflow during data processing. A low pass-filter was needed to reduce the noise of the derivative norm.

5. Preparation for creating evidence layers

Mineral-prospectivity mapping is used to delineate targets potentially containing ore mineralization based on spatial correlation of geological features with known ore deposits (Fallon et al., 2010). Mineral-exploration modelling was used to analyze spatial signatures between known deposits and geological features to establish recognition criteria on a regional scale. Some recognition criteria could be observed directly, whereas some were hidden in the data. In this section, methods of mathematical geology were used to set up the recognition criteria on a regional scale and to create evidence layers for calculating posterior probability.

5.1. Lithostratigraphy

Zhuxi-type polymetallic deposits have a strong spatial and genetic correlation with Carboniferous-Permian lithologic unit with a banded distribution. The mineralization was controlled by NE-trending faults (Fig. 5), and thrust nappe structures protected the Carboniferous-Permian strata beneath the surface from erosion over geologic time, while also reducing the extent of their outcropping at the surface. Buffer analysis and t-test were used to determine the optimum spatial association between mineral deposits and Carboniferous-Permian formations. The t-test result (Fig. 6) showed that the t-values in the area with <1400 m buffer distance were greater than 1.96, which indicated that the strata with 1400 m buffer would make a favorable evidence layer for mineral prospectivity.

5.2. Structure

Geological structure is an important predictive variable and provides the pathway and space for mineral deposition. In the study area, NE-trending faults provided the fluid pathways and controlled the geological framework and thus the ore-deposits distribution. NE-trending faults were overprinted by E-W or NE trending faults. The intersections of these two faults trends created favorable places for granite intrusion and ore deposits. Buffering analysis was used to determine the controlling field of faults. It showed that all deposits were in the 800 m buffering range. The t-test ($\geq$2.36) indicates that the ore deposits have a strong spatial association with the faults (Fig. 7). Therefore, the 800 m buffering range of faults was selected as the evidence layer.

5.3. Granites

Granite intrusions have several outcrops occurring mainly in the southwestern part of Taqian-Fuchun basin. Geophysical interpretation and drilling have proved that there are larger intrusive plutons at depth. The t-values of granites buffering were greater than 1.96 (Fig. 8), which indicates a strong spatial correction between intrusive granites and mineral deposits. When $t > 4$, the cumulative area delineated by the 2000 m buffering range covered 22% of the study area. It was appropriate to delineate the mineral target as the evidence layer.

5.4. Geophysical anomalies

The ground magnetic-survey data were reduced to the pole before detailed geological interpretation. Magnetic highs could be interpreted as indicating areas of intrusive granites. Ore deposits are located at the boundaries of the granites, which reflect high gradients in the magnetic field. The derivative norm of magnetic data was used to highlight areas having high magnetic gradients. The derivative norm map (Fig. 9) and t-test (Fig. 10) show a strong spatial correlation between the derivative norm and ore deposits. Considering the range of cumulative area delineated by the derivative norm and spatial association, we set 0.033 as the threshold value to create the evidence layer.

5.5. Geochemical anomalies

In terms of ore-forming processes, fault systems provide the fluid pathway and space. Therefore, mineral deposits have a high spatial correlation with faults system. In this work, SWPCA and the singularity method were used to extract integrated anomalies for the evidence layer. First, seven principal components were obtained by SWPCA. Principal component variances and component loadings of variables of indictor elements are shown in Fig. 11. The First Principal Component (PC1) accounted for 32.86% of the total variance. Thus, it contained the maximum information of geochemical data and was applied to delineate integrated anomalies.

In the secondary environment, tungsten minerals are usually stable and difficult to be weathered. Minerals of copper, lead and

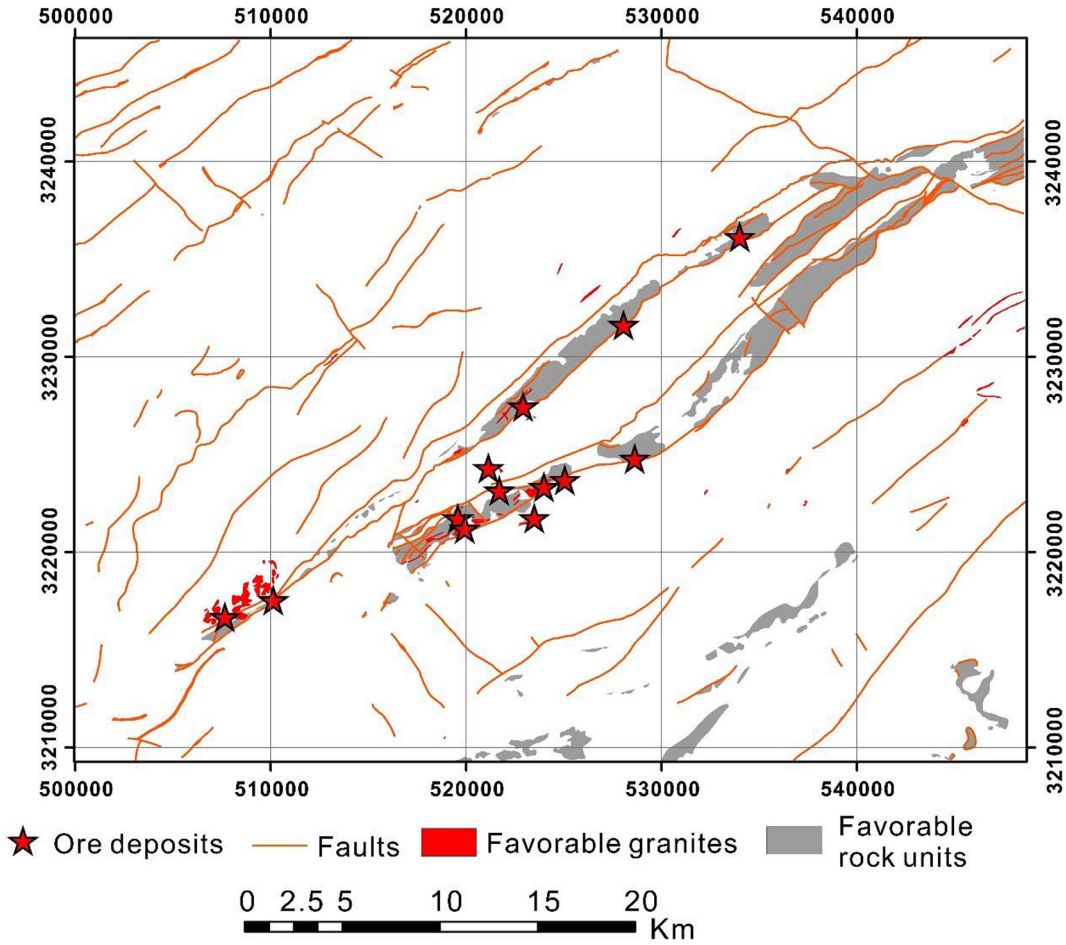

Fig. 5. Simplified geological map of the TFJD study area, showing the spatial relationship of faults, favorable rock units, granites and ore deposits (or occurrences).

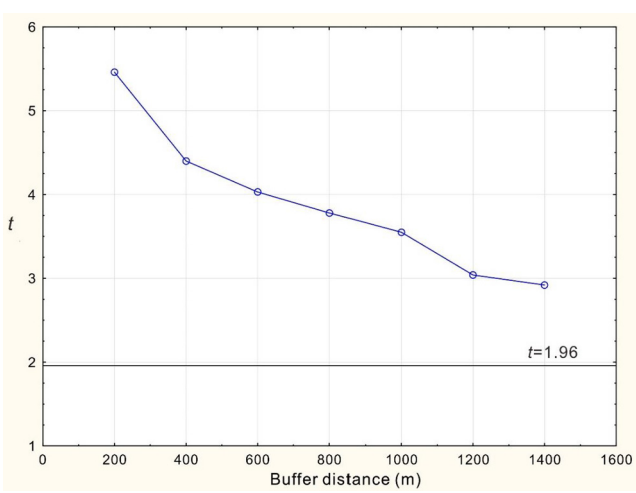

Fig. 6. Plot of *t*-test for determining the spatial relationship between the strata controlling range and ore deposits *vs* the buffering distance. The $t = 1.96$ solid line is regarded as the threshold above which the correlation can be considered as statistically significant.

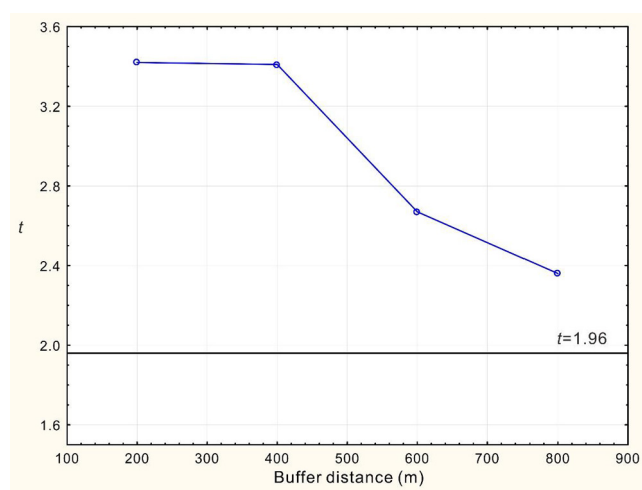

Fig. 7. Plot of *t*-test for determining the spatial relationship between faults and ore deposits *vs* the buffering distance. The $t = 1.96$ solid line is regarded as the threshold above which the correlation can be considered to be statistically significant.

zinc are in the form of sulfide. These sulfides are easily oxidized and broken down, and then copper, lead and zinc can migrate and become secondarily enriched. Tungsten is a high-temperature ore-forming element, whereas copper, lead and zinc are moderate- to low-temperature ore-forming elements. In the Zhuxi orefield, hydrothermal-vein type copper, lead, and zinc orebodies at shallow depths are more easily weathered than copper and tungsten deposits at depth. Therefore, the tungsten loading is not large enough for PC1.

The singularity method was used to enhance integrated geochemical anomalies. In conventional geochemical-data processing,

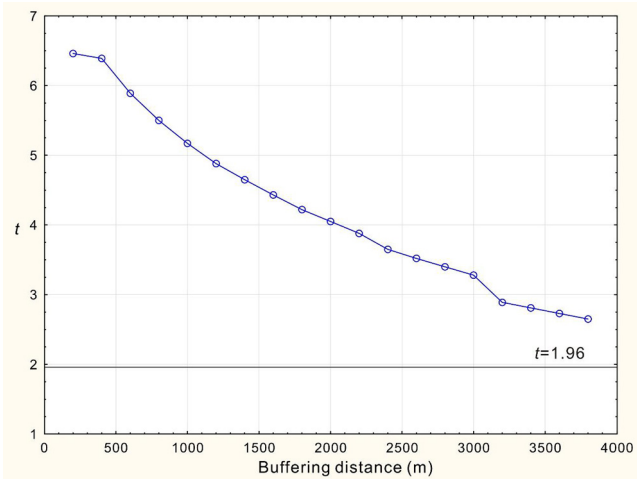

Fig. 8. Plot of *t*-test for determining the spatial relationship between intrusive granites controlling range and ore deposits *vs* the buffering distance. The $t = 1.96$ solid line is regarded as the threshold above which the correlation can be considered to be statistically significant.

a high concentration for an element indicates high probability for a mineral deposit. The higher the element concentration, the greater the *t*-values will be, but for the singularity method, the lower the singularity index α, the greater the *t*-values will be (Fig. 12) and thus the *t*-value curve is descending in Fig. 13. Most known ore deposits are located in areas with singularity index (α) values < 2. The patterns of α values clearly show spatial correlation with singularity anomaly. There was an inflection point in the *t*-test (Fig. 13) from 1.91 to 1.96 of singularity index. Thus, we set $\alpha = 1.91$ as the threshold value to create the evidence layer.

5.6. Regional-scale recognition criteria

Mineral systems and mineral deposit models form the basis to define recognition criteria for regional exploration (Asadi et al., 2015; Chen et al., 2007; Porwal et al., 2010; Xiao et al., 2007). To define the recognition criteria for the Zhuxi-type copper-tungsten polymetallic deposits on a regional scale in the study area, the key geological features (i.e., lithostratigraphy and faults), geochemical anomalies, and magnetic anomalies associated with mineral deposits were determined. The recognition criteria (Table 1) were used to extract the favorable evidence layers used as input to the WofE modelling for delineating prospectivity targets.

6. Results and discussion

The input evidence layers for WofE for integrated prospectivity mapping were extracted based on recognition criteria shown in Table 1. The cell size was usually determined based on the geological complexity, research level, and data scale. In this study, the cell size, based on the data scale, was set to be 500 × 500 m. The posterior probabilities were calculated by GeoDAS software (Cheng, 2000). The cumulative proportions of ore deposits and area (Fig. 14), delineated by posterior probability were 57.89% and 1.16% at a posterior probability of 0.2, respectively. When posterior

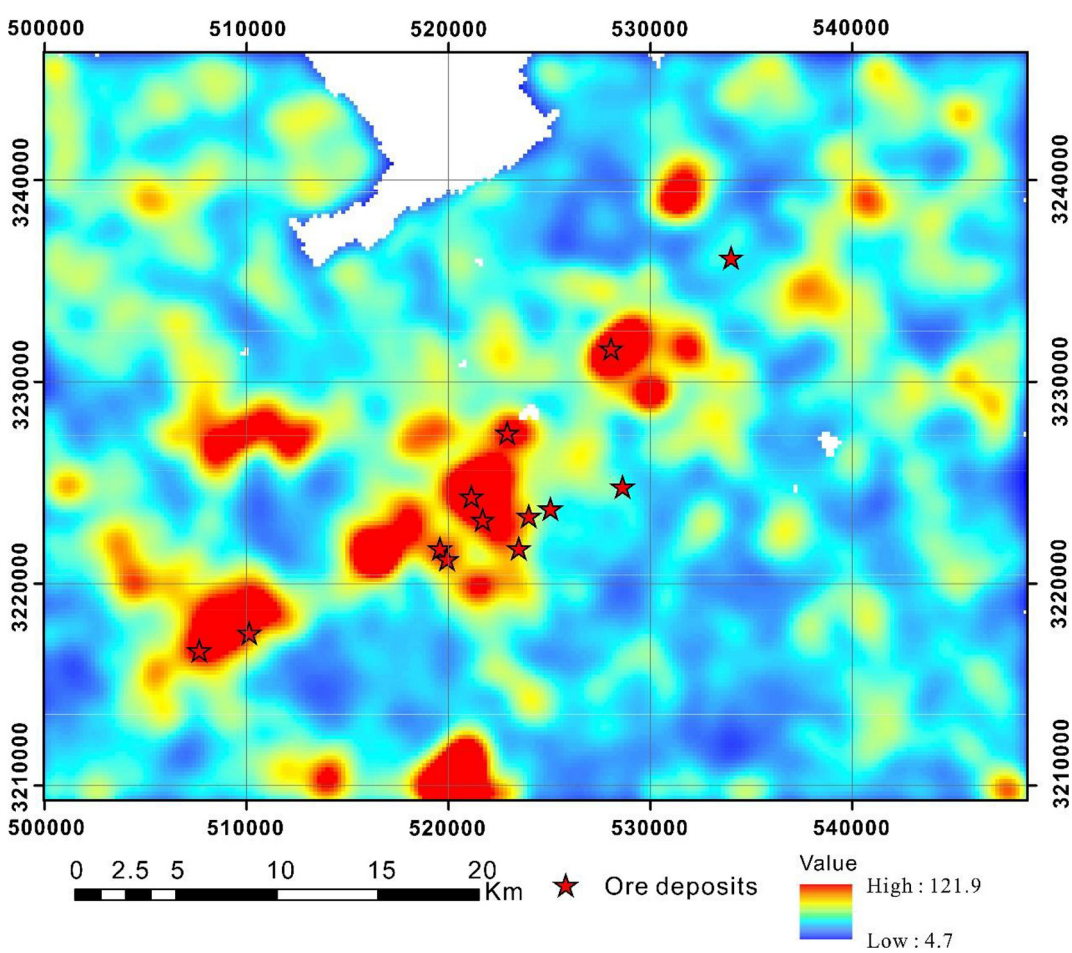

Fig. 9. Mapping of magnetic derivative norm. High values highlight the magnetic field gradient.

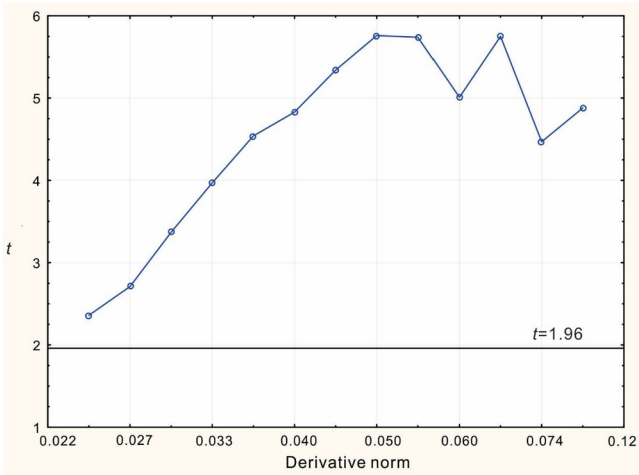

Fig. 10. Plot of *t*-test for determining the optimal threshold values for the derivative norm used to grade geophysical anomalies. The $t = 1.96$ solid line is regarded as the threshold above which the correlation can be considered to be statistically significant.

probability was 0.018, the cumulative proportion of ore deposits reached 100%, while cumulative proportion of area reached 11.05%. Thus, these two posterior probabilities (0.018 and 0.2) were used to divide the posterior probability values into three intervals, corresponding to high potential, moderate potential, and background, respectively. The prospectivity mapping using these two parameters is shown in Fig. 15.

The regional prospectivity mapping confirmed that there is potential for Zhuxi-type polymetallic mineralization. The prospectivity targets (Fig. 15) are in the Taqian-Fuchun basin and have a strong spatial correlation with faults, strata, intrusive granites, geochemical anomalies, and geophysical anomalies, which revealed that the extracted evidence layers contributed significantly to prospectivity mapping of WofE. All known deposits fall into the area with high posterior probability values. This confirmed that the highlighted areas delineated by high posterior probability have much higher potentiality for key breakthroughs in future mineral exploration, especially for areas with high posterior probability where no deposits have yet been found.

In many previous studies, Student's *t*-values not only contained values greater than 1.96, but also contained some values less than 1.96 (Xiao et al., 2012, 2017; Zuo, 2011). We found all the values were greater than 1.96 (Figs. 6–8 and 10) in this study. We could account for this pattern from the perspectives of geology and mathematics. The geology map (Fig. 5) shows that the mineral deposits have a strong spatial correlation with fault, granite, and favorable strata. All the mineral deposits are near the faults, granites, and favorable lithologies. For example, all the mineral deposits are within the 800 m fault buffering range. If the buffering distance

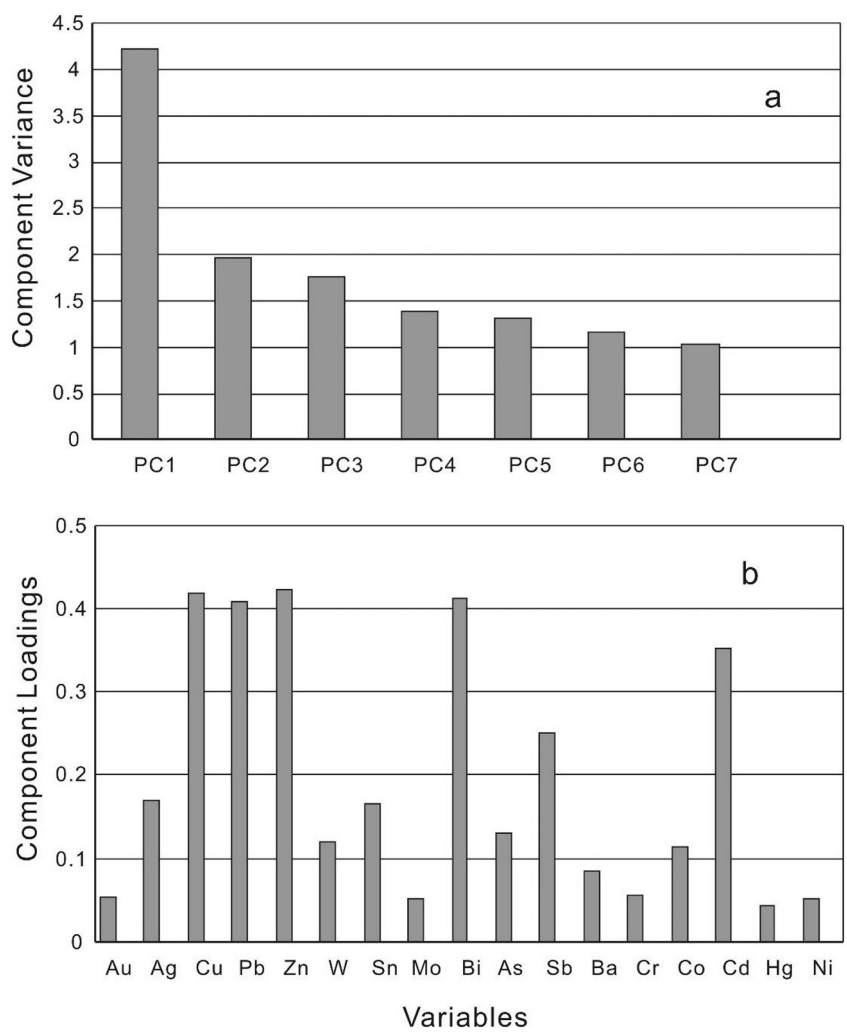

Fig. 11. Results obtained by SWPCA. (a) Component variances of the seven principal components (PCs) and (b) component loadings of variables on the first component (PC1).

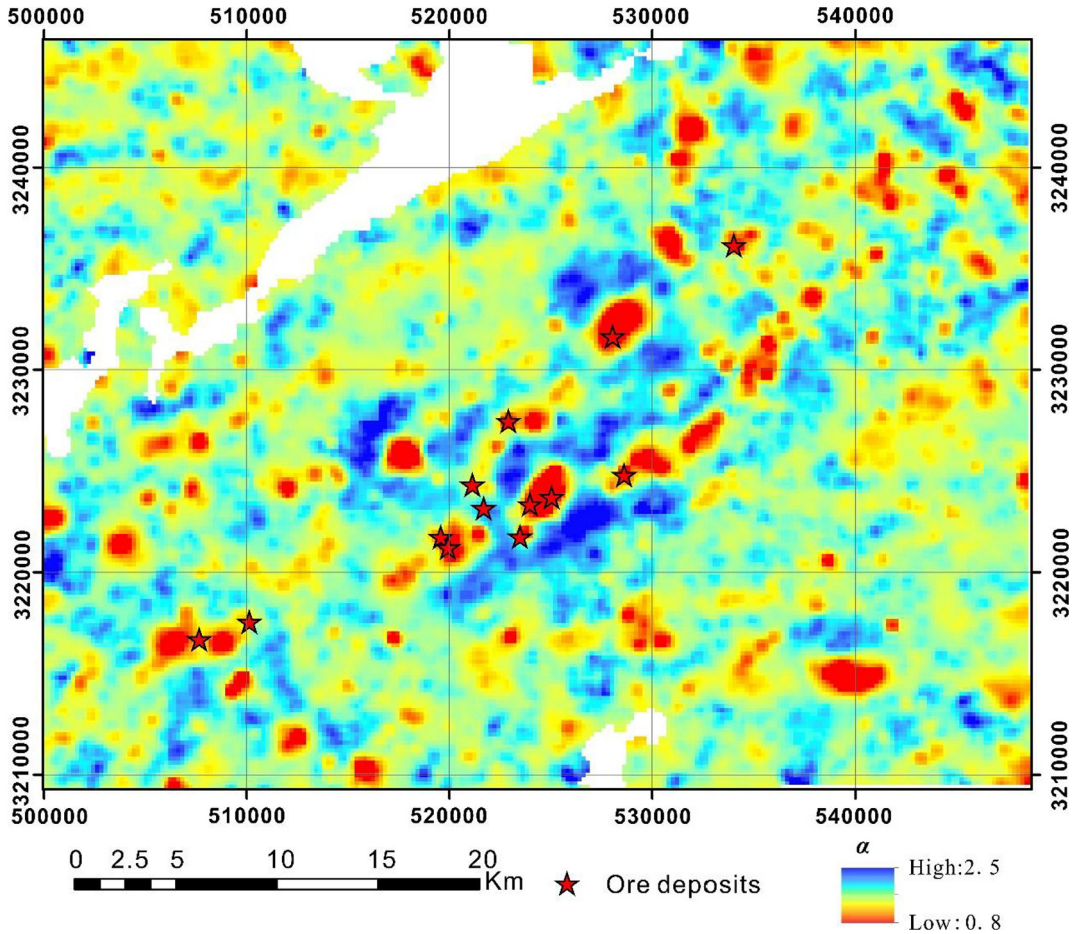

Fig. 12. Singularity mapping of the first principal component of SWPCA. Cell size is 500 × 500 m.

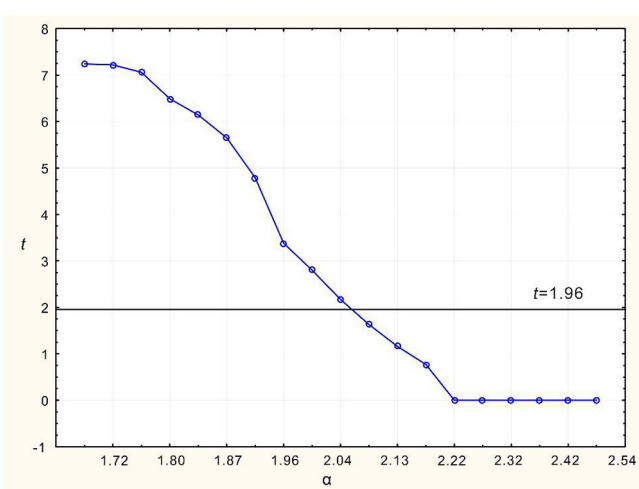

Fig. 13. Plot of t-test to determine the optimal singularity threshold values to use to grade geochemical anomalies. The $t = 1.96$ solid line is regarded as the threshold above which the correlation can be considered to be statistically significant.

were greater than 800 m, the n(M) in Eqs. (1) and (2) would be set to 0, and the t-value would be null. Overall, t-values greater than 1.96 indicate strong spatial correlation between ore deposits and favorable geological features, proving that the favorable geological variables we selected for mineral-prospectivity mapping in this study are appropriate and successful.

Table 1
Regional-scale recognition criteria for Zhuxi-type mineral deposits.

Exploration Criterion	Details
Lithostratigraphy	Carboniferous-Permian strata with 1400 m buffering
Fault	800 m buffering
Granite	Granites with 2000 m buffering
Geophysical anomalies	Derivative norm ≥0.033
Geochemical anomalies	α of integrated geochemical anomalies ≤1.91

In this work, conditional independence was not tested in the WofE model. Violation of the conditional independence assumption can increase posterior probabilities until they approach 1, which implies that there is a 100% chance for successful mineral exploration (Porwal et al., 2010). This is unscientific and has the effect of decreasing the likelihood of exploration success. From the perspective of mathematics theory of WofE, the χ^2 test and the Omnibus test have all been proposed to validate conditional independence of evidence layers (Agterberg and Cheng, 2002; Bonham-Carter, 1994). However, it is unrealistic to assume independence of evidence layers in geology because of the internal spatial and genetic relationships among different geological features. Xiao et al. (2007) proposed a partial correlation coefficient and matching factor methods to evaluate the variables importance for mineral deposits rather than conditional independence. Thus, we avoided discussion related the conditional independence of input evidence layers in our study. The posterior probabilities of WofE could be interpreted as relative estimation for mineralization potential and target areas.

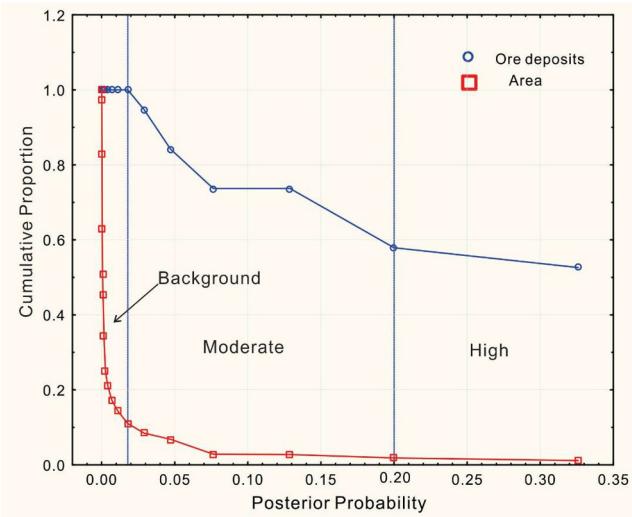

Fig. 14. Cumulative proportions of ore deposits and area delineated by posterior probability. The solid blue lines grade the posterior probability into high potential, moderate potential, and background.

7. Conclusions

The well-known copper-tungsten mineralization is in a Neopaleozoic shallow marine carbonate-rock basin in the northeastern part of Jiangnan Orogen in Jiangxi Province in South China. The Zhuxi deposit is a typical deposit and the world's largest tungsten deposit in the study area. It comprises two main ore zones and some scattered small orebodies, consisting of skarn-type, altered-granite type, and hydrothermal-vein type deposits. The mineralization has a significant zonation and is dominated by hydrothermal-vein type copper, lead, and zinc mineralization at shallow depths; by skarn-type copper and tungsten mineralization at intermediate depths; and by altered-granite-type copper and tungsten mineralization ate depth. Wall-rock alteration caused significant alteration zonation from intrusive granites to the carbonate rocks.

The Zhuxi-type Cu-W polymetallic deposits are hosted in Carboniferous-Permian limestone. NE-trending faults provided the fluid pathways and controlled the geological framework and ore-deposits distribution. Fault intersections were favorable places for granite intrusion and ore deposition. Intrusive S-type granites, dated at 152.9–146.9 Ma, provided the thermal energy and the source material for ore deposition and displayed a strong spatial relationship with the mineral deposits.

Favorable geological information extraction and GIS-based data-integration methods were used extensively for mineral-prospectivity mapping of Zhuxi-type polymetallic deposits. The singularity method is a powerful method that was used to enhance and delineate geochemical anomalies. The derivative norm method was effective for extracting magnetic-gradient anomalies for mineral deposits associated with intrusive granites. The student's *t*-test of WofE was useful to select variables for evidence layers

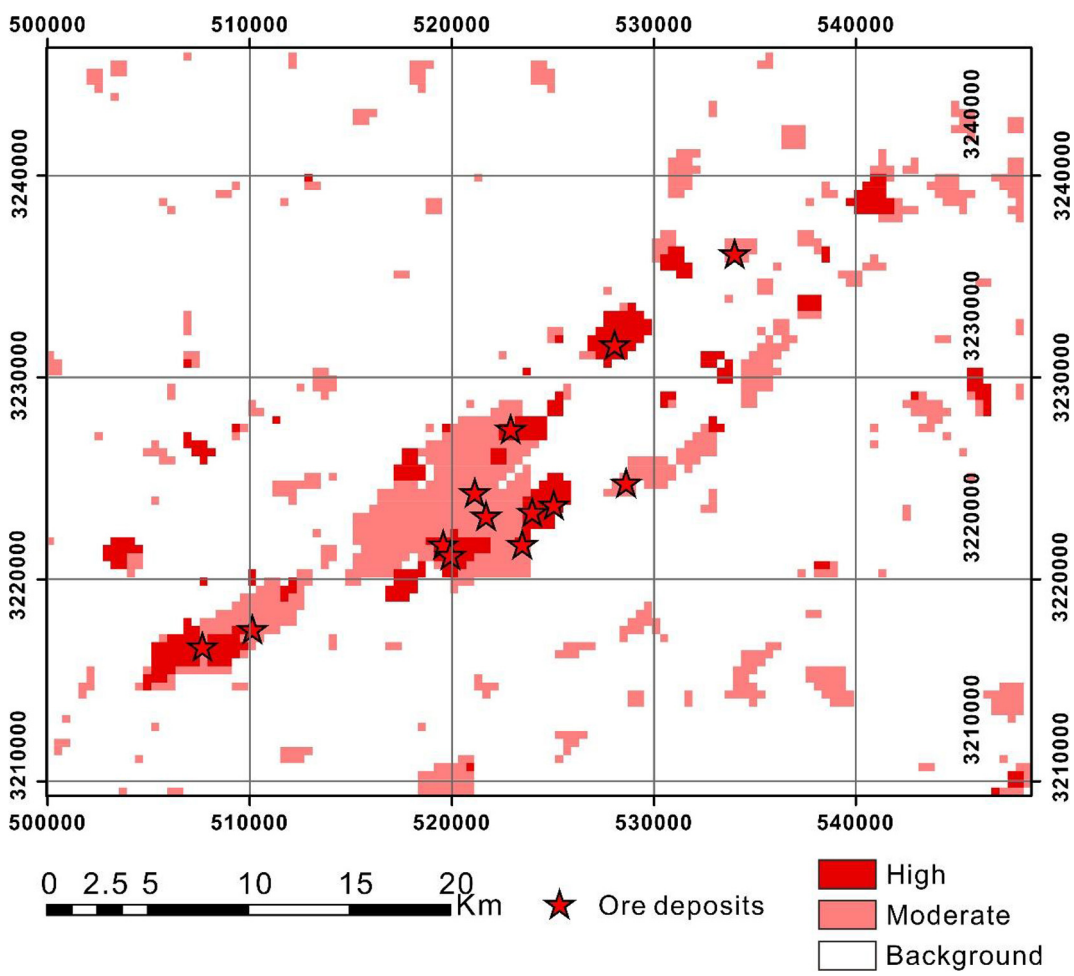

Fig. 15. Prospectivity mapping for Zhuxi-type mineral deposits.

by evaluating the spatial correlation between known deposits and evidence layers.

The posterior probabilities of WofE gave a relative estimation for mineralization potential. The prospectivity mapping confirmed that there is significant potential for Zhuxi-type hydrothermal polymetallic mineralization. Area highlighted by high posterior probability had much greater potential for key breakthroughs in mineral exploration, especially for areas with high posterior probability but where no deposits have yet been found.

Acknowledgments

The authors sincerely thank Dr. Franco Pirajno and three anonymous reviewers for their critical reviews and constructive comments which have improved the manuscript. This research has been financially supported by Chinese Geological Survey Program (12120113065300), Welfare Research Program of Ministry of Land and Resources, PRC (201411035), National Key Technology R&D Program (No. 2011BAB06B08-2) and National Training Program of Innovation and Entrepreneurship for Undergraduates (201610491027).

Appendix A. Supplementary data

Supplementary data associated with this article can be found, in the online version, at http://dx.doi.org/10.1016/j.oregeorev.2017.05.022. These data include Google maps of the most important areas described in this article.

References

Abedi, M., Norouzi, G.H., Fathianpour, N., 2013. Fuzzy outranking approach: a knowledge-driven method for mineral prospectivity mapping. Int. J. Appl. Earth. Obs. 21, 556–567.
Agterberg, F.P., Cheng, Q., 2002. Conditional independence test for weights-of-evidence modeling. Nat. Resour. Res. 11, 249–255.
Agterberg, F.P., Bonham-Carter, G.F., Wright, D.F., 1990. Statistical pattern integration for mineral exploration. In: Gaal GaM, Daniel, F. (Eds.), Computer Applications in Resource Estimation Prediction and Assessment for Metals and Petroleum. Pergamon Press, Oxford, New York, pp. 1–21.
Agterberg, F.P., Bonham-Carter, G.F., Cheng, Q., Wright, D.F., 1993. Weights of evidence modeling and weighted logistic regression in mineral potential mapping. In: Davis, J.C., Herzfeld, U.C. (Eds.), Computers in Geology. Oxford University Press, New York, pp. 13–32.
Andrada de Palomera, P., van Ruitenbeek, F.J.A., Carranza, E.J.M., 2014. Prospectivity for epithermal gold–silver deposits in the Deseado Massif, Argentina. Ore Geol. Rev. 71, 484–501.
Asadi, H.H., Porwal, A., Fatehi, M., Kianpouryan, S., Lu, Y.J., 2015. Exploration feature selection applied to hybrid data integration modeling: Targeting copper-gold potential in central Iran. Ore Geol. Rev. 71, 819–838.
Bonham-Carter, G.F., 1994. Geographic Information Systems for Geoscientists: Modeling With GIS. Pergamon, New York.
Carranza, E.J.M., 2008. Geochemical Anomaly and Mineral Prospectivity Mapping in GIS. Elsevier.
Carranza, E.J.M., 2009. Objective selection of suitable unit cell size in data-driven modeling of mineral prospectivity. Comput. Geosci. 35, 2032–2046.
Carranza, E.J.M., Hale, M., 1997. A catchment basin approach to the analysis of reconnaissance geochemical-geological data from Albay Province, Philippines. J. Geochem. Explor. 60, 157–171.
Carranza, E.J.M., Laborte, A.G., 2014. Data-driven predictive mapping of gold prospectivity, Baguio district, Philippines: application of Random Forests algorithm. Ore Geol. Rev. 71, 777–787.
Chen, Y.Q., Xia, Q.L., Huang, J.N., Chen, J.G., Li, 2007. Application of the weights-of-evidence method in mineral resource assessments in the southern segment of the "Sanjiang metallogenic zone", southwestern China. Chin. Geol. 34, 132–141 (in Chinese with English abstract).
Chen, G.H., Wan, H.Z., Shu, L.S., 2012. An analysis on ore-controlling conditions and geological features of the Cu-W polymetallic ore deposit in the Zhuxi area of Jingdezhen, Jiangxi Province. Acta Petrol. Sin. 28, 3901–3914 (in Chinese with English abstract).
Chen, G.H., Shu, L.S., Shu, L.M., Zhang, C., Ouyang, Y.P., 2015. Geological characteristics and mineralization setting of the Zhuxi tungsten (copper) polymetallic deposit in the Eastern Jiangnan Orogen. Sci. China Earth Sci. 45, 1799–1818 (in Chinese with English abstract).
Cheng, Q., 2000. GeoData Analysis System (GeoDAS) for Mineral Exploration: User's Guide and Exercise Manual. Material for the Training Workshop on GeoDAS Held at York University: York University, p. 204.
Cheng, Q., 2006a. Singularity-generalized self-similarity-fractal spectrum (3S) models. Earth Sci.: J. China U. Geosci. 31, 337–348 (in Chinese with English abstract).
Cheng, Q., 2006b. Spatial and spatially weighted principal component analysis for images processing. Int. Geosci. Remote Sensing, 972-5.
Cheng, Q., 2007. Mapping singularities with stream sediment geochemical data for prediction of undiscovered mineral deposits in Gejiu, Yunnan Province, China. Ore Geol. Rev. 32, 314–324.
Cheng, Q., 2008. Non-Linear Theory and Power-Law Models for Information Integration and Mineral Resources Quantitative Assessments. Progress in Geomathematics: Springer, pp. 195–225.
Cheng, Q., Bonham-Carter, G., Wang, W., Zhang, S., Li, W., Xia, Q., 2011. A spatially weighted principal component analysis for multi-element geochemical data for mapping locations of felsic intrusions in the Gejiu mineral district of Yunnan, China. Comput. Geosci. 37, 662–669.
China Geological Survey, 2010. Mineral Prospecting Technical Requirements in China Geological Survey Work Standards (in Chinese).
Fallon, M., Porwal, A., Guj, P., 2010. Prospectivity analysis of the Plutonic Marymia Greenstone Belt, Western Australia. Ore Geol. Rev. 38, 208–218.
Gao, L., Yang, M., Ding, X., Liu, Y., Liu, X., Ling, L., et al., 2008. SHRIMP U-Pb zircon dating of tuff in the Shuangqiaoshan and Heshangzhen groups in South China-constraints on the evolution of the Jiangnan Neoproterozoic orogenic belt. Geol. Bull. China 27, 1744–1751 (in Chinese with English abstract).
Gao, L., Huang, Z., Ding, X., Liu, Y., Pang, J., 2012. Zircon SHRIMP U-Pb dating of Xiushui and Majianqiao Formations in northwestern Jiangxi Province. Geol. Bull. China 31, 1086–1093 (in Chinese with English abstract).
Han, Y., Zhang, C., Zhang, H., You, G., Li, L., 2016. Configuration of Mid-Neoproterozoic Arc-Basin System in Eastern Jiangnan Orogenic Belt. Geol. Rev. 62, 285–299 (in Chinese with English abstract).
Hu, Z., 2015. The Formation Conditions and Matallogenic Regularity of Zhuxi Tungsten Polymentallic Deposit in Northeast of Jiangxi Province CNKI (China National Knowledge Infrastructure). Chengdu University of Technology (in Chinese with English abstract).
Hua, R., Chen, K., Zhao, l., 1993. Geochemlcal gold depleted zone around the Yinshan ore district, Jiangxi Province, and its metallogenic significance. Miner. Deposits 12, 289–296 (in Chinese with English abstract).
Huang, L., Jiang, S., 2014. Highly fractionated S-type granites from the giant Dahutang tungsten deposit in Jiangnan Orogen, Southeast China: geochronology, petrogenesis and their relationship with W-mineralization. Lithos 202–203, 207–226.
Jiang, Y., Jiang, S., Zhao, K., Ling, H., 2006. Petrogenesis of Late Jurassic Qianlishan granites and mafic dykes, Southeast China: implications for a back-arc extension setting. Geol. Mag. 143, 457–474.
Li, S., He, T., 2016. Jiangxi found the world's largest tungsten mine and achieved four major breakthroughs. Earth, 66–67 (in Chinese).
Li, X.H., Mcculloch, M.T., 1996. Secular variation in the Nd isotopic composition of Neoproterozoic sediments from the southern margin of the Yangtze Block: evidence for a Proterozoic continental collision in southeast China. Precambrian Res. 76, 67–76.
Li, Y., Sheng, J., Bel, L.L., Giuliani, G., 1986. Evidence for the lower continental crustal origin of the Xihuashan Granite. Acta Geol. Sin. 60, 47–64.
Li, Y., Pan, X., Zhao, M., Chen, G., Zhang, T., Liu, X., et al., 2014. LA-ICP-MS Zircon U-Pb Age, Geochemical Features and Relations to the W-Cu Mineralization of Granitic Porphyry in Zhuxi Skarn Deposit, Jingdezhen, Jiangxi. Geol. Rev. 60, 693–708 (in Chinese with English abstract).
Lindsay, M.D., Betts, P.G., Ailleres, L., 2014. Data fusion and porphyry copper prospectivity models, southeastern Arizona. Ore Geol. Rev. 61, 120–140.
Liu, J., He, X., Wan, H., Chen, G., Luo, Z., Yang, X., et al., 2013. Prominent features of Zhuxi copper deposit and the discovery of giant mineral deposit in Jiangxi Province. The Proceedings of the 2013 Annual Conference of the Chinese Geological Society, pp. 275–281 (in Chinese).
Liu, Y., Cheng, Q., Xia, Q., Wang, X., 2014a. Mineral potential mapping for tungsten polymetallic deposits in the Nanling metallogenic belt, South China. J. Earth Sci. China 25, 689–700.
Liu, Z., Liu, S., Chen, Y., Wang, C., Wan, H., Chen, G., et al., 2014b. LA-ICP-MS Zircon U-Pb Isotopic Dating of Lamprophyre Located Zhuxi Copper-Tungsten Mine of Jiangxi Province and Its Geological Significance. Rock Miner. Anal. 33, 758–766 (in Chinese with English abstract).
Lusty, P.A.J., Scheib, C., Gunn, A.G., Walker, A.S.D., 2012. Reconnaissance-Scale Prospectivity Analysis for Gold Mineralisation in the Southern Uplands-Down-Longford Terrane, Northern Ireland. Nat. Resour. Res. 21, 359–382.
Mao, J.W., Xie, G.Q., Li, X.F., Zhang, C.Q., Mei, Y.X., 2004. Mesozoic large scale mineralization and multiple lithospheric extension in South China. Front. Earth Sci. 11, 45–55 (in Chinese with English abstract).
Mao, J., Xie, G., Guo, C., Chen, Y., 2007. Large-scale tungsten-tin mineralization in the Nanling region, South China: metallogenic ages and corresponding geodynamic processes. Acta Pet. Sin. 23, 2329–2338.
Mao, J., Cheng, Y., Chen, M., Pirajno, F., 2012. Major types and time–space distribution of Mesozoic ore deposits in South China and their geodynamic settings. Miner. Deposita. 48, 267–294.
Mao, Z., Cheng, Y., Liu, J., Yuan, S., Wu, S., Xiang, X., et al., 2013. Geology and molybdenite Re–Os age of the Dahutang granite-related veinlets-disseminated tungsten ore field in the Jiangxin Province, China. Ore Geol. Rev. 53, 422–433.

Peng, J., Zhou, M.F., Hu, R., Shen, N., Yuan, S., Bi, X., et al., 2006. Precise molybdenite Re–Os and mica Ar–Ar dating of the Mesozoic Yaogangxian tungsten deposit, central Nanling district, South China. Miner. Deposita. 41, 661–669.
Porwal, A., González-Álvarez, I., Markwitz, V., McCuaig, T.C., Mamuse, A., 2010. Weights-of-evidence and logistic regression modeling of magmatic nickel sulfide prospectivity in the Yilgarn Craton, Western Australia. Ore Geol. Rev. 38, 184–196.
Rodriguez-Galiano, V., Sanchez-Castillo, M., Chica-Olmo, M., Chica-Rivas, M., 2015. Machine learning predictive models for mineral prospectivity: an evaluation of neural networks, random forest, regression trees and support vector machines. Ore Geol. Rev. 71, 804–818.
Shu, L., Shi, Y., Guo, L., Charvet, J., Sun, Y., 1995. The Late Proterozoic Plate Tectonics and Collisional Kinematics in the Middle Part of the Jiangnan Belt. Nanjing University Publishing House, Nanjing (in Chinese).
Shu, L., Faure, M., Wang, B., Zhou, X., Song, B., 2008. Late Palaeozoic-Early Mesozoic geological features of South China: Response to the Indosinian collision events in Southeast Asia. C. R. Geosci. 340, 151–165.
Su, X., 2014. Geology, Geochemistry of Zhuxi Tungsten Copper Deposit in Jingdezheng, Jiangxi Province CNKI (China National Knowledge Infrastructure). China University of Geosciences, Beijing (in Chinese with English abstract).
Wan, D., 1995. Geochemical Anomaly Features of the Fujiawu Porpbgry Copper (Molybdenum) Depesit, Jianxi Province. Geol. Prospect. 1, 47–51 (in Chinese with English abstract).
Wan, H., Liu, Z., Liu, S., Chen, Y., Wang, C., Chen, G., et al., 2015. LA-ICP-MS Zircon U-Pb Dating of Granodioritic Porphyry located Zhuxi Copper-Tungsten Mine in Northeast Jiangxi and Its Geological Significance. Rock Miner. Anal. 34, 494–502 (in Chinese with English abstract).
Wang, D., Shu, L., 2012. Late Mesozoic basin and range tectonics and related magmatism in Southeast China. Geosci. Front. 3, 109–124.
Wang, Q., Zi, F., 2007. Partial Melting of Thickened or Delaminated Lower Crust in the Middle of Eastern China: Implications for Cu-Au Mineralization. J. Geol. 115, 149–161.
Wang, X., Zhou, J., Qiu, J., Zhang, W., Liu, X., Zhang, G., 2006. LA-ICP-MS U-Pb zircon geochronology of the Neoproterozoic igneous rocks from Northern Guangxi, South China: Implications for tectonic evolution. Precambrian Res. 145, 111–130.
Wang, X., Zhao, G., Zhou, J., Liu, Y., Hu, J., 2008. Geochronology and Hf isotopes of zircon from volcanic rocks of the Shuangqiaoshan Group, South China: Implications for the Neoproterozoic tectonic evolution of the eastern Jiangnan orogen. Gondwana Res. 14, 355–367.
Wang, X., Shu, L., Xing, G., Zhou, J., Tang, M., Shu, X., et al., 2012. Post-orogenic extension in the eastern part of the Jiangnan orogen: Evidence from ca 800–760 Ma volcanic rocks. Precambrian Res. 222–223, 404–423.
Wang, C., Chen, J., Zhang, Z., Xiao, F., Wu, G., 2013. Metallogenic characteristics and quantitative prediction of hydrothermal Pb-Zn-Ag polymetallic ore deposits in northwest Zhejiang. J. Geol. (China) 37, 436–443 (in Chinese with English abstract).
Wang, Y., Xue, C., Liu, J., Wang, J., Yang, J., Zhang, F., et al., 2015. Early Carboniferous adakitic rocks in the area of the Tuwu deposit, eastern Tianshan, NW China: Slab melting and implications for porphyry copper mineralization. Asian Earth Sci. 103, 332–349.
Wei, X., 1996. The Geological Characteristics of Jinshan Ductile Shear Zone-Type Gold Deposit in Jiangxi. Geol. Jiangxi. 10, 52–64 (in Chinese with English abstract).
Wu, X., Lou, F., Liu, C., Zhao, L., 2005. Establishment of the Wannian Group in the Wannian area, northeastern Jiangxi, China and its significance. Geol. Bull. China. 24, 819–825 (in Chinese with English abstract).
Wu, X., Ouyang, Y., Zhou, Y., Zhong, S., Chen, G., 2015. Geochemical characteristics of magmatite and their constraints on mineralization of the Zhuxi tungsten-copper polymetallic deposit in Jingdezhen, Jiangxi Province. Geol. China 42 (6), 1885–1896 (in Chinese with English abstract).
Xi, Y., Liao, H., 1997. A Study on the Prmaty Enrichment trendency of Gold in Presinian Strata of the Northeast Jiangxi Area. Geol. Jiangxi. 1, 46–51 (in Chinese with English abstract).
Xiao, K., Zhang, X., Li, J., Yang, Y., Chen, J., Ding, J., et al., 2007. Quantitative assessment method for national important mineral resources prognosis. Front. Earth Scis. 14, 20–26 (in Chinese with English abstract).
Xiao, K., Lou, D., Yang, Y., Li, J., 2009. Typical models of National total mineral prediction. Institute of Mineral Resources, Chinese Academy of Geological Sciences, pp. 1–61. (in Chinese).
Xiao, F., Chen, J., Zhang, Z., Wang, C., Wu, G., Agterberg, F.P., 2012. Singularity mapping and spatially weighted principal component analysis to identify geochemical anomalies associated with Ag and Pb-Zn polymetallic mineralization in Northwest Zhejiang, China. J. Geochem. Explor. 122, 90–100.
Xiao, F., Chen, J., Hou, W., Wang, Z., Zhou, Y., Erten, O., 2017. A spatially weighted singularity mapping method applied to identify epithermal Ag and Pb-Zn polymetallic mineralization associated geochemical anomaly in Northwest Zhejiang. China. J. Geochem. Explor.
Xu, B., Guo, L., Shi, Y., 1992. Proterozoic Terranes and Multiphase Collision Orogens in Anhui-Zhejiang-Jiangxi Area. Geological Publishing House, Beijing (in Chinese).
Yang, M., Mei, Y., Zhou, Z., 1998. Ore-Forming Rule and Prospecting of the Luoxiao-Wuyi Uplift and Chenzhou-Shangro Depression. Geological Publishing House, Beijing (in Chinese).
Yang, M., Huang, S., Lou, F., Tang, W., Mao, S., 2009. Lithospheric structure and large-scale metallogenic process in Southeast China continental area. Chin. Geol. 36, 528–543 (in Chinese with English abstract).
Zhao, G., 2015. Jiangnan Orogen in South China: developing from divergent double subduction. Gondwana Res. 27, 1173–1180.
Zhao, G., Cawood, P.A., 1999. Tectonothermal evolution of the Mayuan Assemblage in the Cathaysia Block: Implications for Neoproterozoic collision-related assembly of the South China Craton. Am. J. Sci. 299, 309–339.
Zhou, X., Sun, T., Shen, W., Shu, L., Niu, Y., 2006. Petrogenesis of Mesozoic granitoids and volcanic rocks in South China: a response to tectonic evolution. Episodes 29, 26–33.
Zhou, J., Wang, X., Qiu, J., 2009. Geochronology of Neoproterozoic mafic rocks and sandstones from northeastern Guizhou, South China: Coeval arc magmatism and sedimentation. Precambrian Res. 2009 (170), 27–42.
Zuo, R., 2011. Identifying geochemical anomalies associated with Cu and Pb–Zn skarn mineralization using principal component analysis and spectrum–area fractal modeling in the Gangdese Belt, Tibet (China). J. Geochem. Explor. 111, 13–22.